Macromolecular and mechanical changes in aged silicones

Thayri Khaled, Agustin Rios de Anda, Emmanuel Richaud

MACROMOLECULAR AND MECHANICAL CHANGES IN AGED SILICONES

Thayri KHALED[1,2], Agustín RIOS DE ANDA[2]*, Emmanuel RICHAUD[1]**

1. Laboratoire Procédés et Ingénierie en Mécanique et Matériaux, Arts et Métiers Sciences and Technologies, CNRS, CNAM, HESAM University,151 bd de l'hôpital, 75013 Paris, France.

2. Université Paris Est Créteil, Institut de Chimie et des Matériaux Paris-Est, 2 rue Henri Dunant, 94320 Thiais, France.

* agustin.rios-de-anda@u-pec.fr

** emmanuel.richaud@ensam.eu

ABSTRACT

Three room temperature-vulcanized rubbers were thermally aged under air at 250°C or submitted to aminolysis at room temperature. Ageing was followed by uniaxial tensile testing, sol gel measurements in toluene, and Time Domain Double Quantum NMR characterization. Mechanical tests were exploited to identify the parameters of the Ogden model so as to describe the hyperelastic behavior of PDMS. Sol gel and Double Quantum NMR were used to track and quantify macromolecular changes within the samples. A multiscale correlation between the results of each technique was proposed to highlight the understanding of multiscale analysis in rubber ageing.

KEYWORDS

Polydimethylsiloxane, thermal ageing, aminolysis, DQ NMR, mechanical behavior

INTRODUCTION

Polydimethylsiloxanes are a set of elastomer polymers which are widely used as insulator coatings or concrete additives due to their hydrophobicity [1], as biomaterials due to their biocompatibility [2], and as sealants due to their resistance to highly polar solvents (alcohols, water, acetonitrile …) or moderately ones (ketones, esters…) [3,4], among other applications. They can be considered as relatively expensive compared to common rubbers (EPDM for instance) yet they still are considered as a commodity material[5], and, as all crosslinked materials, they are almost impossible to recycle, which makes necessary to increase their lifetime.

The chemical mechanisms of degradation have been extensively studied by several authors like as Grassie [6], Camino [7] among others [8,9]. By combining TGA analyses in anisothermal or isothermal mode, and analyses of VOC release, two main mechanisms were highlighted: thermal depolymerisation (also named unzipping) occurring in chain ends and/or randomly and thermal oxidation.

The effect of ageing has been also investigated at a macromolecular scale [10,11] in particular for radio-oxidative ageing. The main complexity for this polymer is the difficulty in the analysis of insoluble networks, in which the glass transition temperature only slightly changes with crosslink density [12,13] in comparison with epoxies for instance [14], leading to a difficult track of either

chain scission or crosslinking variation. Crosslinking trackers such as the decrease on crystallization are easy to follow but hard to exploit in the absence of well-established quantitative relationships. As such, Time Domain Double Quantum (DQ) ^{1}H NMR appears as a pertinent tool since it can directly measure a variation on crosslink density through chain scission, and can thus link such variation to the distribution of molar mass between crosslinks [15,16]. Moreover, DQ NMR yields also the crosslink density distribution, the percentage of free and dangling chains and the relaxation times of elastically-bond chains, and their evolution with ageing. As such, this technique can give valuable intrinsic structural information not available from other macroscopic techniques such as swelling or mechanical characterizations. Furthermore, the great advantage of using this method in PDMS is that there is no need to overheat samples (with subsequent in situ degradation) since they are already in the elastic rubbery domain at room temperature.

At macroscopic scale, despite existing works of the modelling of elastic behavior in PDMS [17], and on the effect of ageing [18,19], they are only few works dealing with the modeling of the effect of ageing on mechanical properties.

Consequently, this paper aims to study the macromolecular change in PDMS networks with controlled level of selective ageing leading specifically to chain scission or crosslinking and propose a set of mechanical behavior laws related with such macromolecular changes. For that purpose, three Room Temperature Vulcanized PDMS differentiated by their initial crosslink density will be studied. They will be aged following two distinct conditions (thermal ageing and aminolysis) expected to have different consequences in terms of macromolecular architecture variation. Ageing will be monitored by mechanical testing and DQ NMR in order to establish a relationship between the evolution of PDMS structure with its ageing. The aim of this work is to complete current literature on this topic. Indeed, such literature discusses mainly the influence of ageing on crosslink density and the evolution of the mechanical behavior. In this work, by taking advantage of all obtained experimental data, we aim to further the understanding and establishing physical correlations between molecular and macroscopic experiences, namely by relating a mechanical elastic model, to the crosslink density distribution and relaxation times obtained by DQ NMR, which has seldomly been considered. Such an approach can readily be applied to other elastomers and thermosets in general.

MATERIALS AND METHODS

1. Materials

Three Room Temperature Vulcanized non-reinforced PDMS were considered in this work. They were supplied by Esprit Composite as bicomponent mixtures, i.e. Part A containing PDMS chains with some Silyl Si-H groups, and Part B containing vinyl ended PDMS chains. Pt catalyst is present in only one of the parts so that reaction starts when part A and part B are mixed. Curing was performed at room temperature according after having mixed part A and part B in equal mass ratios. The reactive mixture was stirred and homogenized for 2 minutes, casted in a Petri dish and cured for 24 h at room temperature. The mass of reactive mixture poured in Petri dish was adjusted to obtain 2 mm-thick samples.

According to supplier data, the shore hardnesses were respectively equal to 10, 33 and 42, confirming their different crosslink density. After curing, samples were punched in order to obtain

ISO 527-2B type samples 15 mm in length on the strain zone, 4 mm width, and 2 mm thick. Given the relatively high permeation of oxygen into PDMS rubbers [20], it will be assumed that samples are homogenously degraded and that there is no DLO effect. This will be tentatively justified by experimental data (see later).

2. Ageing conditions

2.1. Thermal ageing

PDMS samples were isothermally aged at 250°C under ambient air in a UF55 plus Memmert ventilated oven with exposure duration varying from 5 hours up to 5 days. 250°C was chosen as a simple manner to accelerate degradation with a predominant crosslinking, as it will be discussed later.

2.2. Aminolysis

PDMS samples were immersed in a solution made of THF/EtOH (50ml/2.5 g), KOH (0.72 g) and N-ethylaniline (0.1 g). Exposures were performed at 25°C for 1 and 2 hours.

3. Characterization

3.1. Sol Gel analysis

Samples (m_0 about 100 mg) were immersed in toluene. After 72 h, the swollen mass $m_{swollen}$ was estimated. This duration was verified to correspond to solvent sorption equilibrium within the materials. Samples were thus left in a hood for the solvent to evaporate, and the mass of dried samples m_{dried} corresponding to the insoluble network was measured after 24 hours of drying. Obtained data were used to estimate the swelling ratio:

$$SR = \frac{m_{swollen}}{m_{dried}} \qquad (1)$$

and the soluble fraction:

$$SF = \frac{m_0 - m_{dried}}{m_0} \qquad (2)$$

3.2. Tensile tests

Uniaxial tensile tests were performed on an Instron 5966 device, equipped with a 10kN sensor load. Tests were performed at a 100 mm min^{-1} elongation rate. At least five samples per formulation per ageing were tested.

3.3. Time Domain DQ ^{1}H NMR

^{1}H Double Quantum DQ experiments were conducted on a Bruker Avance III 400 NMR equipped with a 5 mm ^{1}H Static probe. These experiments are based on Baum–Pines pulse sequences [21,22] optimized by Saalwächter [23,24,25,26,27,28,29,30], Lorthioir [31,32]. Such experiments yield two components as a function of the DQ evolution time τ_{DQ}: the DQ buildup I_{DQ} and the reference decay I_{ref}. **Figure 1a** shows an example of such signals. The full magnetization of the sample I_{TOT} corresponds to the sum of I_{DQ} and I_{ref}, and comprises the response of both the dipolar coupled network and the uncoupled mobile network defects such as dangling or free chains. These fractions are characterized by different types of relaxation behavior. Chains fully belonging to the network relax faster and non-exponentially, whereas dangling and free (i.e. non-elastic) chains exhibit a slower exponential relaxation.

As described previously [33,34,35,36,37,38,39,40,41,42], in order to properly get access to the network structure, DQ experiments must be undertaken in the temperature-independent regime, i.e. the probed molecular motions must be effective in the fast motion regime. All DQ NMR measurements carried out on all PDMS were conducted at 23°C, at least 90°C above their presumed glass transition temperature T_g of -120°C. These ensures that all tests are carried out in the fast motion regime.

In this temperature-independent regime, to discriminate the network structure influence on the DQ build-up, a normalization of this signal has to be carried out. This normalized signal I_{nDQ} is calculated according to Eq. 3 and it must reach a plateau at the value 0.5 [36,37,38].

$$I_{nDQ} = \frac{I_{DQ}}{I_{ref}+I_{DQ}-I_{def}} \qquad (3)$$

This normalization (i.e. Eq. 3) considers the subtraction of the non-elastic chains I_{def} (i.e. dangling or free chains) contribution from the total signal. A heuristic approach readily allowing the identification and subtraction of this contribution is to fit I_{def} through a double exponential from the $I_{ref} - I_{DQ}$ v.s. τ_{DQ} signal [15,27,36]. Extrapolating this I_{def} fit to τ_{DQ} = 0 gives the percentage of defects (i.e. non-elastic chains) w_{def}. An example of this approach is given in **Figure 1a**.

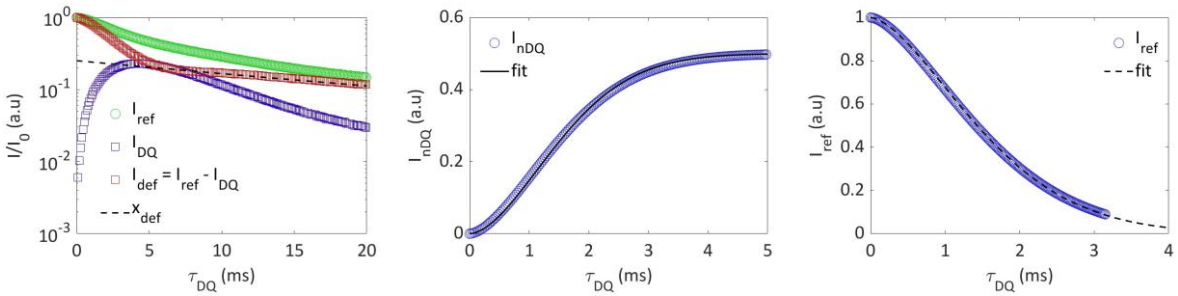

(a) (b) (c)

Figure 1. ^{1}H DQ NMR I_{ref}, I_{DQ}, $I_{ref} - I_{DQ}$, and I_{def} signals vs τ_{DQ} obtained for the Shore 33 PDMS. The contribution from defects I_{def} is emphasized in the $I_{ref} - I_{DQ}$ signal as the fraction of the signal with a long relaxation time (dashed black curve). Extrapolation of the Idef signal to τ_{DQ} = 0 gives the fraction of defects w_{def} (a) Normalized I_{nDQ} signal for the Shore 33 PDMS obtained from Eq. 3 and fitted with Eq. 5 to compute the numerical D_{res} value (b). I_{ref} signal for the Shore 33 PDMS fitted by Eq. 7 to obtain τ and b (c).

Moreover, I_{nDQ} gives access to the residual dipolar coupling D_{res} related to the network structure. In turn the local average dynamic segmental orientation parameter S_b is deduced using Eq. 4, in which D_{stat} is the static coupling constant, D_{res} the residual dipolar coupling, and k a correction factor related to intersegmental motions. The key point is that S_b is directly related to the intrinsic structure of the polymer network via R, the average end-to-end vector between cross-links or equivalently via N, the number of statistical segments between crosslinks. b is the statistical segment length. By considering that $R^2 = Nb^2$ as for ideal chains, S_b should be proportional to 1/N, or equivalently to the cross-links density $v_C = 1/M_C$ as detailed in Eq. 4 .

$$S_b = k\frac{D_{res}}{D_{stat}} \approx \frac{R^2}{N^2 b^2} \approx \frac{1}{N} \propto \frac{1}{M_C} \propto v_C \qquad (4)$$

To obtain the D_{res} value for each sample, each I_{nDQ} signal was fitted by a function detailed in Eq. 5, up to $I_{nDQ} = 0.48$:

$$I_{nDQ} = 0.5\left[1 - exp\left(-(D_{res}\,\tau_{DQ})\right)^n\right] \qquad (5)$$

where n is an exponent varying between 1 and 2. The closer n is to the value of 2, the more homogeneous the network is. **Figure 1b** shows an example of such a fit for the Shore 33 PDMS. Moreover the D_{res} values distribution was obtained by considering a Tikhonov approach [35]. As the k factor and the value of D_{stat} are known for PDMS, the crosslink density measured by ^{1}H DQ NMR $\nu_{C\text{-}NMR}$ can be calculated from Eq. 6 [15] and compared to th value computed from mechanical tests.

$$\nu_{C-NMR} = \frac{D_{res}/2\pi}{1.225\ kHz} \qquad (6)$$

Finally, through an Anderson-Weiss approach [43,44], the relaxation times of the elastic chain domains τ were calculated by fitting the I_{REF} signal decay in the elastic chains region with a compressed exponential as detailed in Eq. 7 where β is a distribution exponential. The closer β is to 2, the relaxation times τ distribution is closer to a normal distribution. An example of such fit is given in **Figure 1c**.

$$I_{ref} = \frac{I}{I_0} = exp - \left(\frac{t}{\tau}\right)^{\beta} \qquad (7)$$

RESULTS

1. Initial characterization

The concentration in elastically active chains $\nu_{C\text{-}FR}$ can be calculated from the Flory Rehner equation [45] in which the correction for phantom network was added since the high solvent uptake induces a large deformation [37]:

$$-[\ln(1-\phi) + \phi + \chi.\phi^2] = V_{m\,toluene}.\nu_{C-FR}.\left(\phi^{\frac{1}{3}} - \frac{2\phi}{f}\right).\frac{f-2}{f} \qquad (8)$$

Where

$$\phi = \frac{1}{1 + \frac{\rho_{polymer}}{\rho_{toluene}}(SR - 1)} \qquad (9)$$

where ν_C is the concentration in elastically active chains (mol l^{-1}), ϕ is the volume fraction of PDMS in the PDMS-toluene swollen mixture, $V_{m\ toluene}$ is the toluene molar volume (106.1 cm^3 mol^{-1}), f is the functionality of PDMS network, and χ is the Flory parameter describing the interaction between PDMS and toluene given by Eq. 10 [46].

$$\chi = 0.459 + 0.134\phi + 0.59\phi^2 \quad (10)$$

The initial characterization of PDMS rubbers is given in **Table 1**.

	SR (Eq. 1)	SF (Eq. 2)	ϕ (Eq. 9)	χ (Eq. 10)	$\nu_{C\text{-}FR}$ (mol l^{-1}) (Eq. 8)
shore 10	4.067-4.094	0.133-0.135	0.203-0.204	0.508	0.037
shore 33	2.848-2.995	0.043-0.045	0.283-0.295	0.544-0.547	0.81-0.86
shore 42	2.432-2.467	0.042-0.044	0.349-0.355	0.572-0.575	0.123-0.128

Table 1. Initial characterization of PDMS under investigation (range mean that data were obtained for triplicates).

It is however complicated to assume that the use of Eq. 8 according to the phantom model will remain valid for aged samples where solvent uptake will be changed by either chain scissions or crosslinking, or that their behavior will be described by the affine model. That is the reason why in the following of this paper, we will only consider swelling ratio or soluble fraction.

Afterwards, the mechanical properties of samples where studied. Obtained stress strain curves are given in Figure 2, displaying the classical hyperelastic behaviour also observed in [47,48], namely an upturn in the high strain domain (300% and above). As it will be discussed later, this means that elastic modulus changes with the deformation level. In other words, it is difficult to describe and link together the architecture of the polymer's network and its elastic modulus, for instance at low strain. More robust trackers are needed which militates, for us, to use robust hyperelastic models such as explained in the Discussion section. It seems however clear that, by observing the tensile test results, there is a clear difference in crosslink density between the three networks considered herein (as also observed in Table 1).

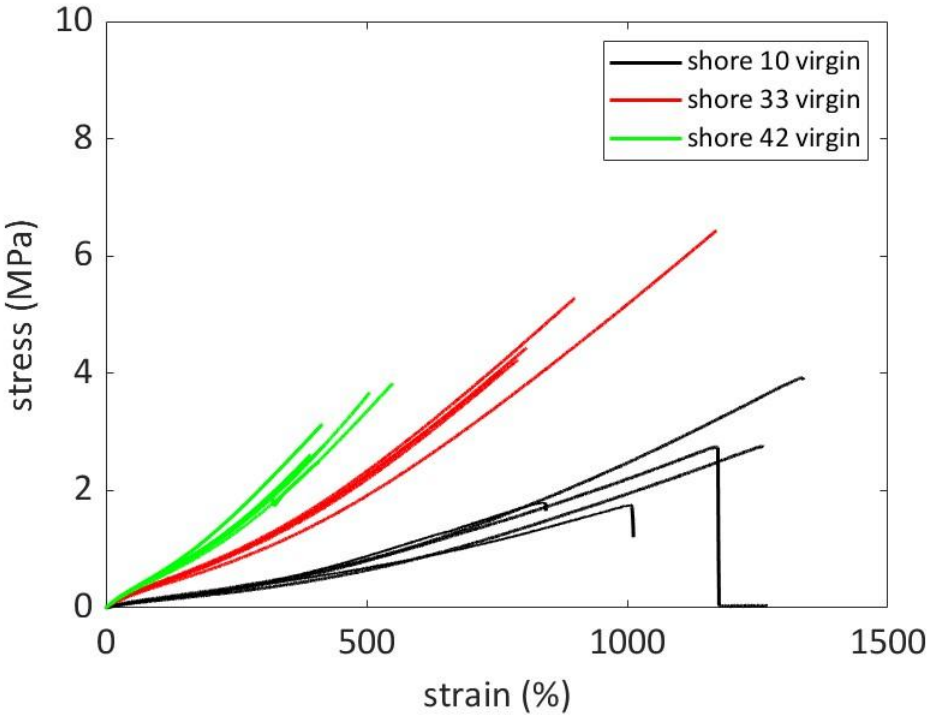

Figure 2. Stress strain curves of unaged PDMS.

The three non-aged PDMS were then characterized by ^{1}H DQ NMR. **Table 2** lists the NMR crosslink densities $\nu_{C\text{-}NMR}$ as well as the relaxation parameters τ and β from Eq. 7. It is seen that the Shore 33 and Shore 42 PDMS have close $\nu_{C\text{-}NMR,}$ τ and b values. This would mean that their crosslink density, as well as the elastic chains mobility and distribution is similar. For the Shore 10 sample, the $\nu_{C\text{-}NMR}$ are lower than for the Shore 33 and Shore 42 PDMS, meaning that this sample is less crosslinked. Moreover for the Shore 10 sample τ is larger and b is smaller than for the Shore 33 and Shore 42 PDMS, meaning that the chains in this sample are more mobile and with a wider relaxation time distribution.

These results are in good agreement with the macroscopic mechanical characterizations. Indeed Shore 10 PDMA has lower moduli and larger elongation at break than Shore 33 and Shore 42 PDMS which is a macroscopic indication of a lower crosslink density at the molecular level.

2. Mechanical characterization of aged samples

Stress strain curves of PDMS after various level of thermal ageing are given in **Figure 3**. They can be commented as follows: the hyperelastic behavior is observed for virgin and aged PDMS, followed by a progressive decrease in ultimate elongation, together with an overall increase in apparent elastic modulus in the short deformation range.

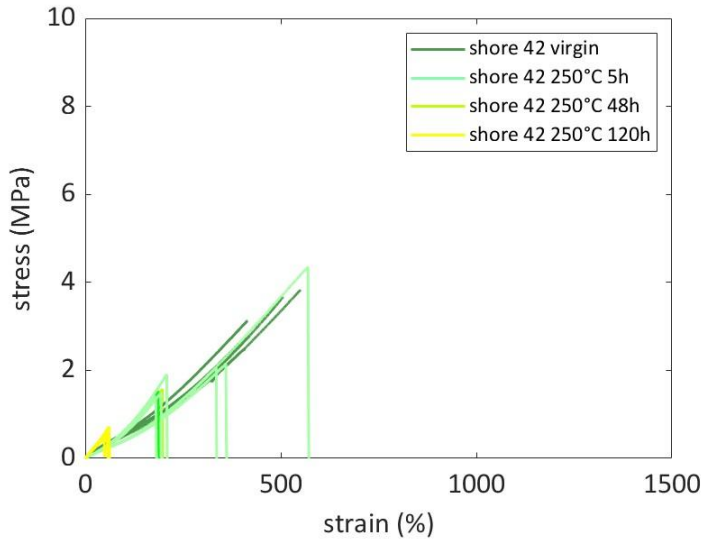

234

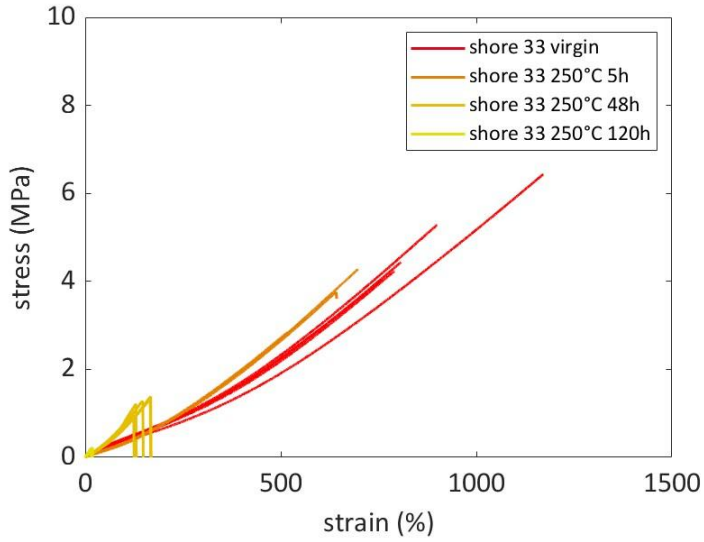

235

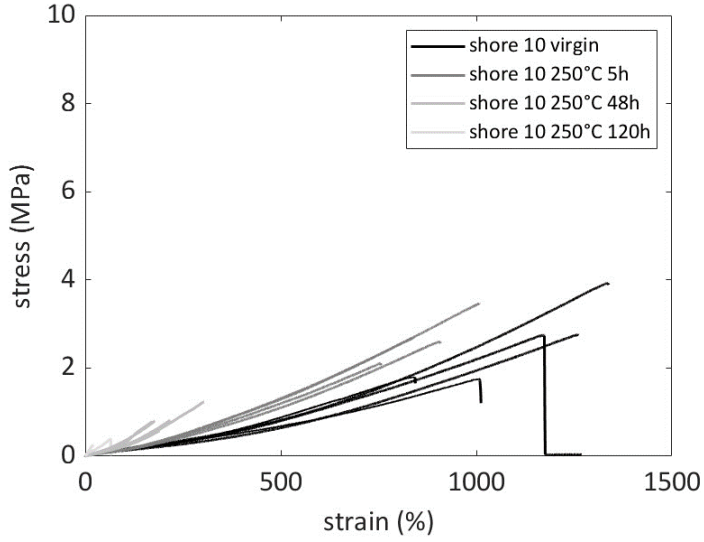

236

237 **Figure 3. Stress strain curves of PDMS before and after thermal oxidation at 250°C under air.**

238

These changes are in accordance with a predominant crosslinking mechanism. This is consistent with the literature, where possible oxidation mechanisms are proposed involving the radical oxidation of methyl group with formation of peroxides (**Scheme 1a**) or the scission of main chain followed by a recombination for instance (**Scheme 1b**).

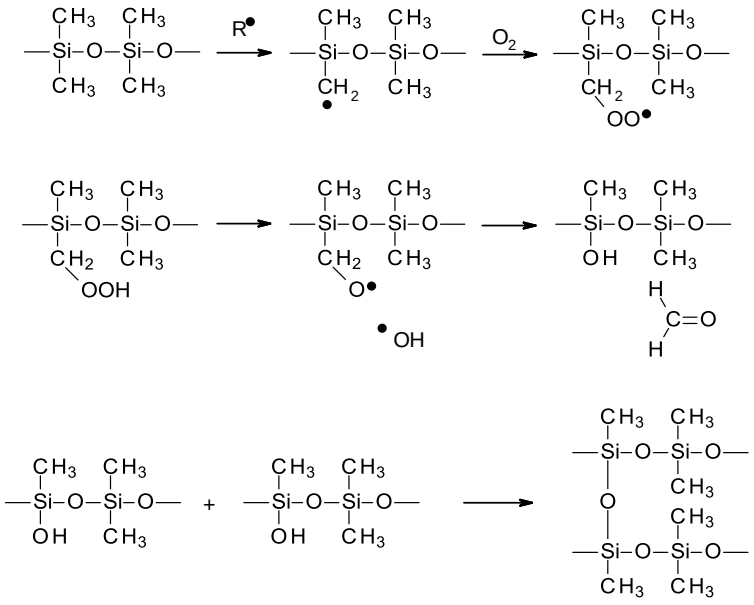

(a)

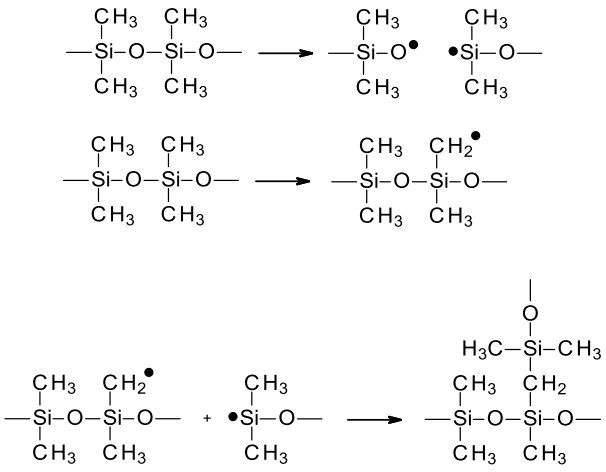

(b)

Scheme 1. Possible thermal oxidation mechanisms [16,49,50,51].

Aminolysis corresponds to a reaction for which a polar species may induce a chain scission process, converting an insoluble network into free soluble chains. This reaction has been studied in the case of tetrafunctional PDMS networks cured with an organostanous catalyst [52,53]. Its effect on the mechanical properties of PDMS is illustrated in Figure 4. Overall, it seems that the hyperelastic behavior is lost, together with an apparent decrease of elastic modulus at low strain.

258

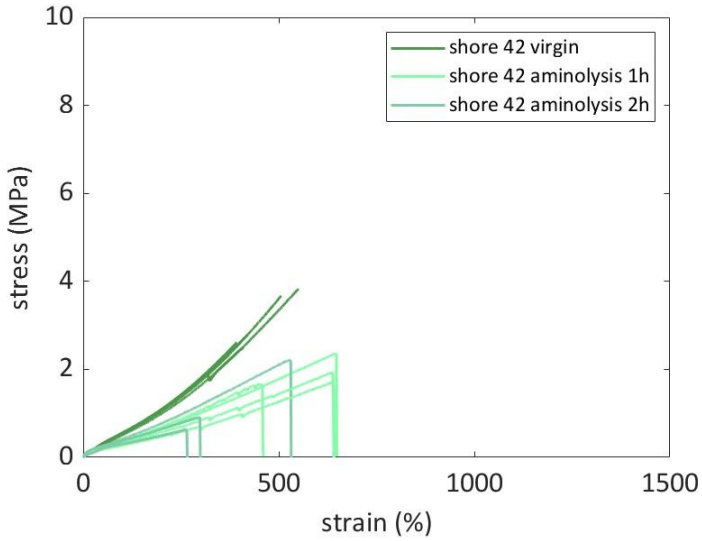

259

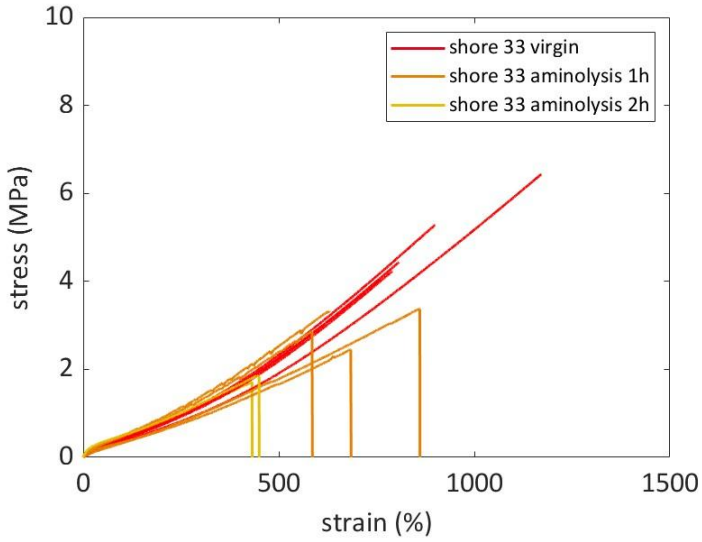

260

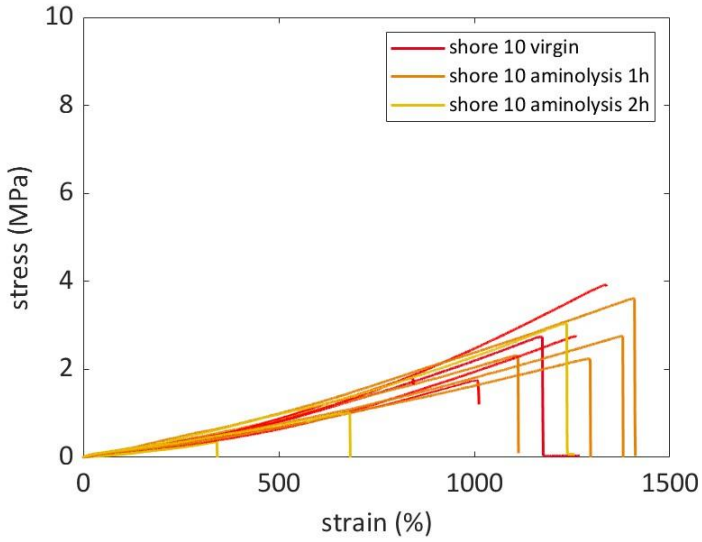

261

Figure 4. Stress strain curves of PDMS before and after aminolysis.

These changes correspond with the well accepted following mechanism: potassium hydroxide and the secondary amine for a cation (Scheme 1 – step 1) can react by a substitution reaction with Si-O groups (Scheme 1 – step 2), inducing a scission of elastically active chains. At the end of the reaction, the secondary amine is regenerated (Scheme 1 – step 3) so that reaction can go on until the degelation of the network, i.e. the loss of all elastically active chains meaning that network turn back to a soluble state. However, the fact that elastically active chains decrease slowly within the first hours of ageing suggests a mechanism occurring rather in the samples' surface than in its bulk.

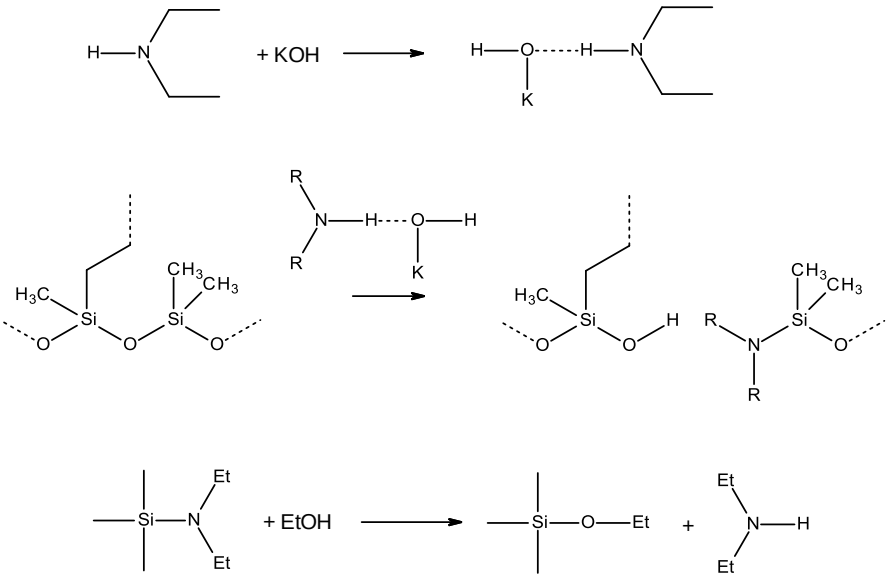

Scheme 2. Mechanisms of aminolysis.

3. Macromolecular characterization of aged samples

The swelling ratio and soluble fractions were measured before and after thermal oxidation. A slight increase is observed at early exposure times, revealing the existence of chain scission process. This one is counterbalanced by a predominant crosslinking process at long ageing times. For aminolysis, the soluble fraction decreases, but this is not surprising since short chains are directly extracted by the liquid media during ageing. Overall, the swelling ratio remains fairly constant, according to the same reasons evoked in the paragraph above.

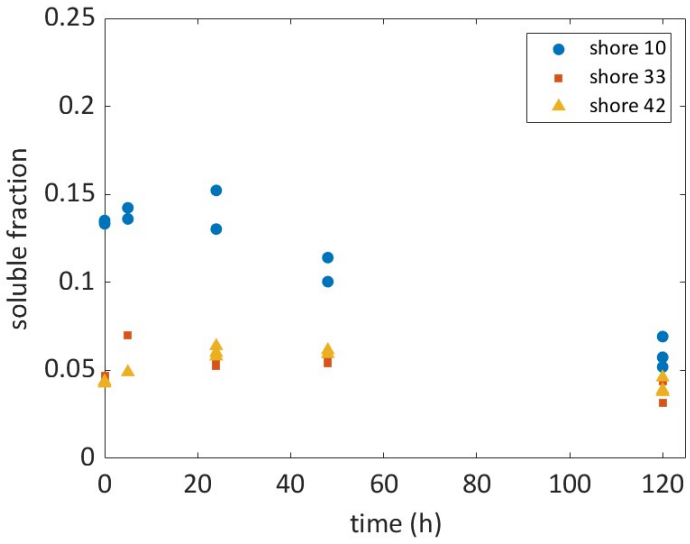

284

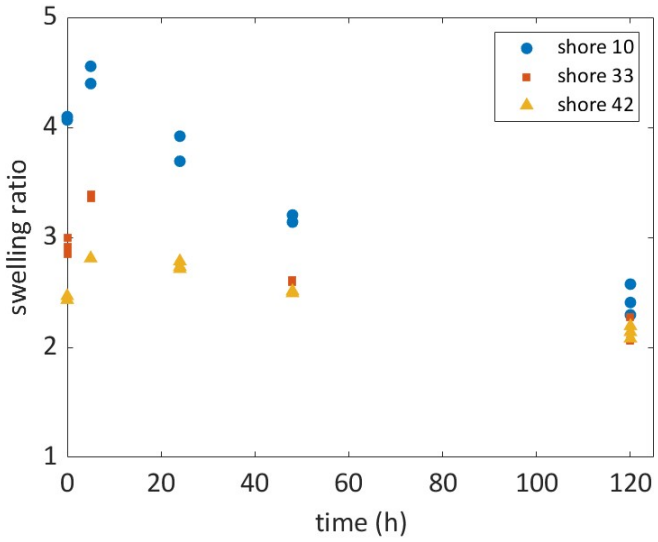

285

286 **Figure 5. Changes in swelling degree (a) and soluble fraction (b) after thermal oxidation at 250°C**
287 **under air.**

288

289

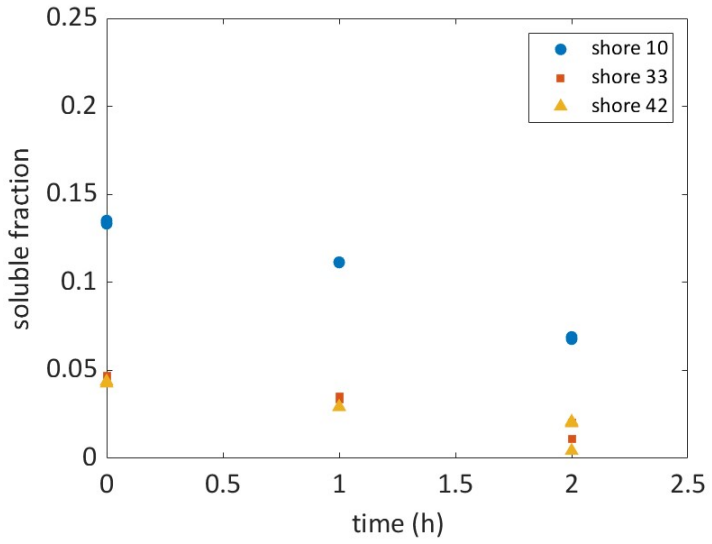

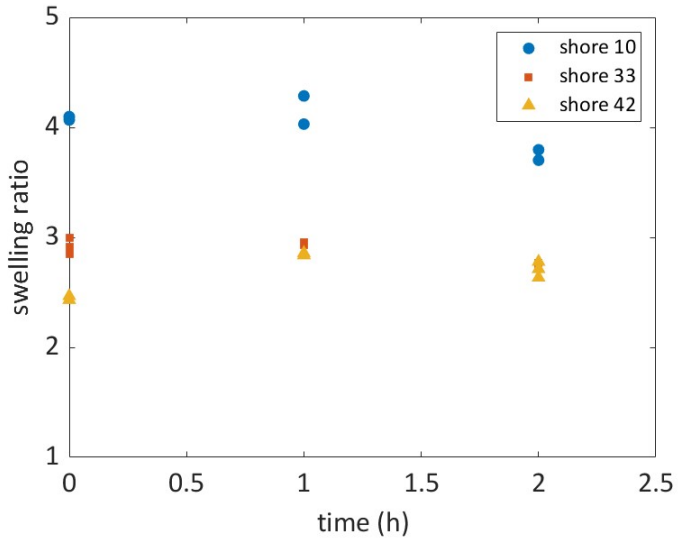

Figure 6. Changes in swelling degree (a) and soluble fraction (b) after aminolysis.

Since exploitation of sol-gel measurement for estimating crosslink density is somewhat tricky, DQ NMR tests were performed. Figure 7 and Table 2 show that in the case of Shore 10 PDMS, thermal aging seems to increase the crosslink density ν_c. This might be due to priming further chemical reactions happening during heating. This is also observed on the elastic chains molecular mobility. Indeed, τ diminishes and b increases, which would lead to think that the mobility decreases as chains become more entangled due to the priming of new crosslink reactions.

In the case of Shore 33 and Shore 42, the increase of ν_c is only observed after 120h thermal aging. It might be possible that at this temperature, both chain scission and chain crosslinking are competing with each other, thus yielding higher crosslink densities compared to the non-aged material. Otherwise, thermal and aminolysis aging leads to chain scission for both PDMS and the longer the aging, the greater the loss in crosslink density. This is accompanied by an increase in elastic chains molecular mobility as observed by the increase on τ with aging time.

Interestingly, ν_C distribution remains relatively narrow compared to comparable data obtained in the case of climatic ageing (which is, in essence, more heterogeneous). We hence believe that there is no DLO effect.

By considering a Tikhonov approach, we were able to calculate the distribution of D_{res} ergo $\nu_{C\text{-}NMR}$ values from ^{1}H DQ NMR data for all studied samples. Figure 8 plots these distributions centered along the mean value for each non-aged PDMS sample, as it is visually easier to differentiate each distribution.

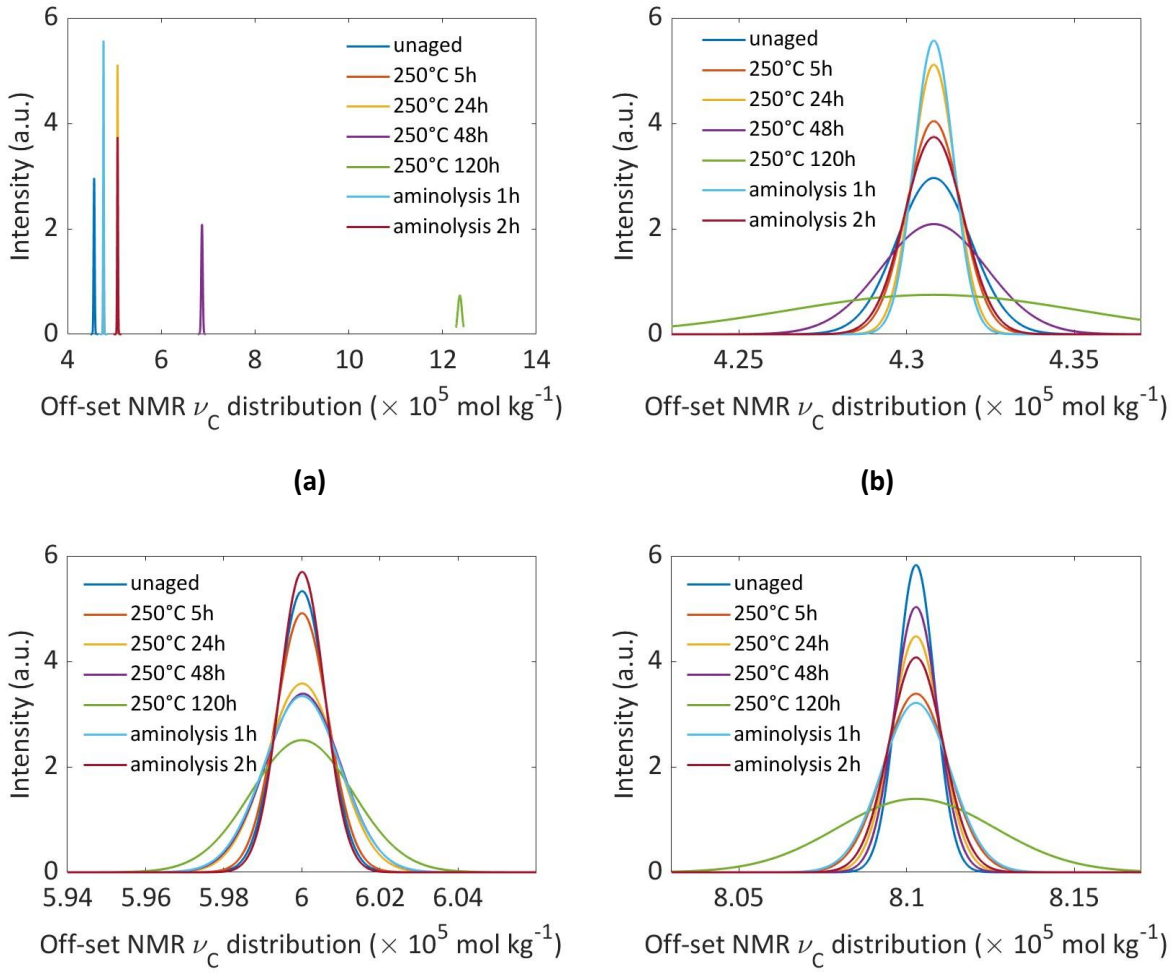

Figure 7. ^{1}H DQ NMR $\nu_{C\text{-}NMR}$ distributions for shore 10 PDMS (a) and data centered along the mean value for each non-aged PDMS sample: raw data for Shore 10 (b), Shore 33 (c) and Shore 42 (d).

Figure 7a plots the absolute $\nu_{C\text{-}NMR}$ distributions for the Shore 10 samples. As it can be seen, a visual difference on distributions cannot be differentiated. Thus, it was decided that the $\nu_{C\text{-}NMR}$ distributions would be centered according to the non-aged sample for a better visualization. This is observed in Figures 7b through 7d.

It can be seen in Figure 7 that the influence of aging for each PDMS on the $\nu_{C\text{-}NMR}$ distribution is distinct among the three studied materials. For Shore 10, it is seen that both thermal aging up until

24h and aminolysis aging yield a narrower $\nu_{C\text{-}NMR}$ distribution. In the case of thermal aging for this material, this could be explained by the fact that $\nu_{C\text{-}NMR}$ increases with aging time, leading to propose that further crosslinks are formed and thus the material becomes less heterogenous. For long thermal aging exposure, chains start to be broken and thus the heterogeneity of the materials increases. In the case of aminolysis, as it is an aggressive aging medium, chains are broken and the crosslink density rapidly diminishes. Yet as chain length diminishes, it tends towards more regular masses, thus yielding a narrower $\nu_{C\text{-}NMR}$ distribution. For Shore 33, the $\nu_{C\text{-}NMR}$ distribution becomes broader with thermal aging and for 1 h aminolysis, as chains are broken, this PDMS inner structure becomes more heterogeneous, thus yielding larger $\nu_{C\text{-}NMR}$ distributions. In the case of 2 h aminolysis, a similar effect as the one described for Shore 10 might explain the narrowing of $\nu_{C\text{-}NMR}$ distribution. Finally, for Shore 42, regardless of aging method or time, the $\nu_{C\text{-}NMR}$ distribution becomes broader with aging time, leading to conclude that for this PDMS, as chains are broken by aging, this material inner chain morphology becomes more heterogeneous.

Sample	Conditionning		Mechanical testing				^{1}H TD-DQ NMR		
			E small def (MPa)	$\nu_{C\text{-}mech}$ = E/3RT small (mol/kg)	$3c_1 + 4.5c_2$ (MPa)	$\nu_{C\text{-}mech}$ = $(3.c_1+4.5c_2)/3RT$ small (mol l^{-1})	$\nu_{C\text{-}NMR}$ (mol l^{-1})	τ (ms)	β
Shore 10	Neat		0.217	0.029	0.207	0.028	0.043	3.76	1.16
	Thermal aging	5h	0.218	0.029	0.299	0.04	0.045	3.89	1.24
		24h	0.150	0.020	0.175	0.024	0.048	3.02	1.15
		48h	0.237	0.032	0.365	0.049	0.066	2.89	1.17
		120h	1.12	0.151	0.77	0.104	0.121	1.33	1.27
	Aminolysis	1h	0.30	0.04	0.246	0.033	0.045	3.57	1.32
		2h	0.29	0.039	0.241	0.033	0.048	2.94	1.37
Shore 33	Neat		0.571	0.077	0.601	0.081	0.06	2.01	1.38
	Thermal aging	5h	0.377	0.051	0.52	0.07	0.059	2.74	1.26
		24h	0.340	0.046	0.413	0.056	0.057	2.74	1.28
		48h	0.744	0.100	0.836	0.113	0.082	1.95	1.30
		120h	1.335	0.180	1.412	0.191	0.125	1.17	1.35
	Aminolysis	1h	0.728	0.098	0.672	0.091	0.068	2.05	1.46
		2h	0.85	0.114	0.746	0.101	0.07	1.78	1.63
Shore 42	Neat		0.723	0.097	0.764	0.103	0.081	1.43	1.34
	Thermal aging	5h	0.532	0.072	0.593	0.08	0.066	2.20	1.31
		24h	0.374	0.050	0.537	0.073	0.068	2.30	1.19
		48h	0.487	0.066	0.845	0.102	0.07	2.28	1.18
		120h	1.094	0.147	1.144	0.155	0.102	1.55	1.25
	Aminolysis	1h	0.577	0.078	0.534	0.072	0.071	1.92	1.51
		2h	0.688	0.093	0.614	0.083	0.07	1.62	1.43

Table 2. Concentration in elastically active chains (Eq. 12) and related values from mechanical and NMR DQ tests.

DISCUSSION

The main aim of this section is to propose a model describing the hyperelastic behavior of PDMS with the minimal number of adjustable parameters, highlighting the changes in macromolecular mobility from DQ NMR data, propose and justify correlations between macromolecular and mechanical testing.

1. Mechanical modelling

The Ogden model [54] was chosen to represent the hyperelastic behaviour of virgin and aged PDMS, which allows the total description of the shape of the curve:

$$\sigma_0 = c_1.\left(\lambda^{\alpha_1-1} - \frac{1}{\lambda^{\frac{\alpha_1}{2}+1}}\right) + c_2.\left(\lambda^{\alpha_2-1} - \frac{1}{\lambda^{\frac{\alpha_2}{2}+1}}\right) + \cdots \qquad (11)$$

Formally, this model is strictly equivalent to the Flory model of affine networks when $c_2 = 0$ and $\alpha_1 = 2$ [55]. In this last case, c_1 directly expresses the entropic elasticity of Gaussian chains connected to two crosslink nodes. Bernardi et al [56] have for instance described the stress and strain curves of unaged PDMS with an Ogden model composed of three terms. Basing on [57], the hyperelastic behavior will be justified as the sum of only two components: one given with $\alpha_1 = 2$ for long elastic chains and the second is characterized by an arbitrary fixed $\alpha_2 = 3$ parameter expressing the presence of shorter chains (possibly created by the thermal induced crosslinking). Its increase would express the occurrence of crosslinking process as explained in the previous paragraph. In this approach, c_2 ($\alpha = 3$) and c_1 ($\alpha = 2$) represent the relative contribution respectively for short chains and long chains. Those coefficients were extracted from a Matlab® routine (see Supplementary Information). In general, very good fits ($R^2 > 0.99$) were obtained (see Supplementary Information). Corresponding c_1 and c_2 values were plotted in Figure 8. As previously observed, in the case of thermal ageing induced crosslinking, long elastically active chains are converted into shorter ones, which corresponds to the right part of Figure 7. In the case of aminolysis, where chain scission must predominate, it is expected that long elastically active chains are converted into some longer elastically active chains, which seems the case

The advantage of using a hyperelastic model is that the whole stress strain curve can be described by c_1 and c_2, which is better than discussing on local elastic modulus values. Considering $\lambda = 1 + \varepsilon$, Eq 9 becomes, at very low strains:

$$E = 3c_1 + \frac{9}{2}c_2 = 3\nu_{C-mech}RT \qquad (12)$$

The estimate of $\nu_{C\text{-}mech}$ is reported in Table 2.

As previously observed in [48], the oxidation induced crosslinking leads to a disappearance of long elastically active chains meanwhile the concentration in elastically active short chains increase, i.e. c1 decreases is correlated to a c_2 increase. For the aminolysis, where presumably chain scission

predominates, the same correlation is also observed (despite the experimental scattering), but this time, ageing results in a c_1 increase (and c_2 decrease).

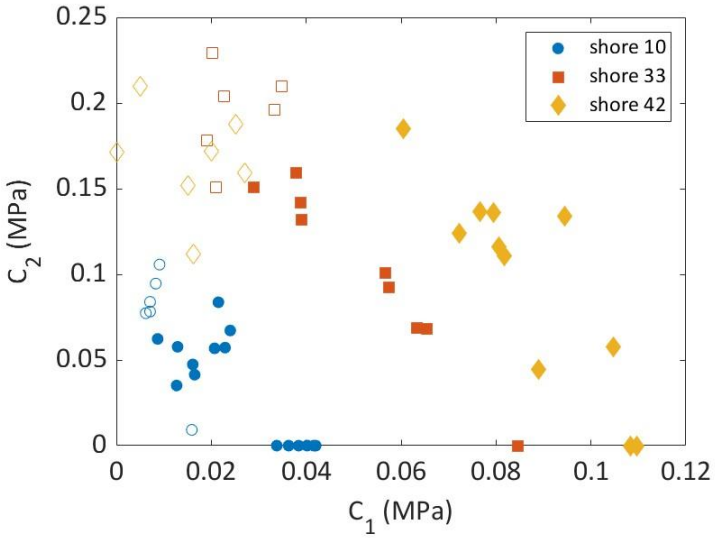

Figure 8. Effect on ageing on the conversion of "long" elastically active chains (expressed by C_1) into short ones (expressed by C_2). Full and open symbols respectively correspond to thermal oxidation and aminolysis.

C_2 quantity was exploited to describe changes in fracture toughness. This latter quantity was estimated from the area under stress strain curve (denoted by W in the following), corresponding to the energy per volume necessary to induce failure. The plot in Figure 9 shows that W first increases with the concentration in short elastically active chains, consistently with previous works [47] but at too elevated concentration in short elastically active chains, the crack propagates catastrophically and sample gets brittle.

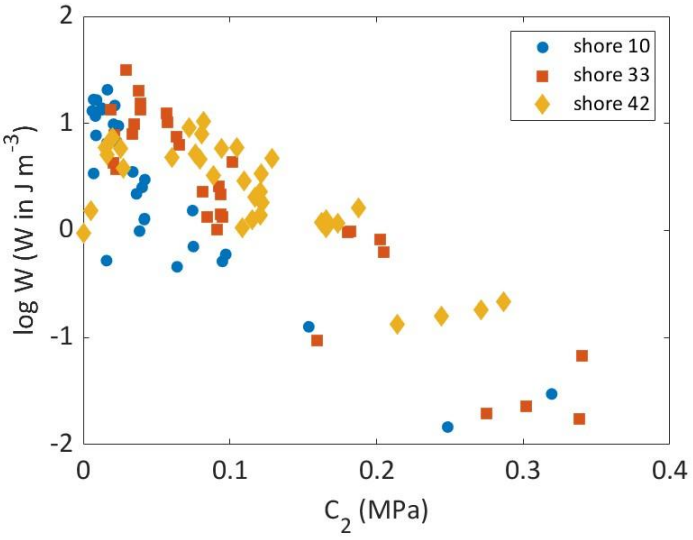

Figure 9. Effect of short chains concentrations expressed by C_2 on toughness expressed by log W.

2. Structure properties relationships

The crosslink density values obtained by mechanical testing for all samples (from Eqs 6 and 12) and all ageing conditions were confronted to those obtained by DQ NMR. This is graphically shown in Figure 10.

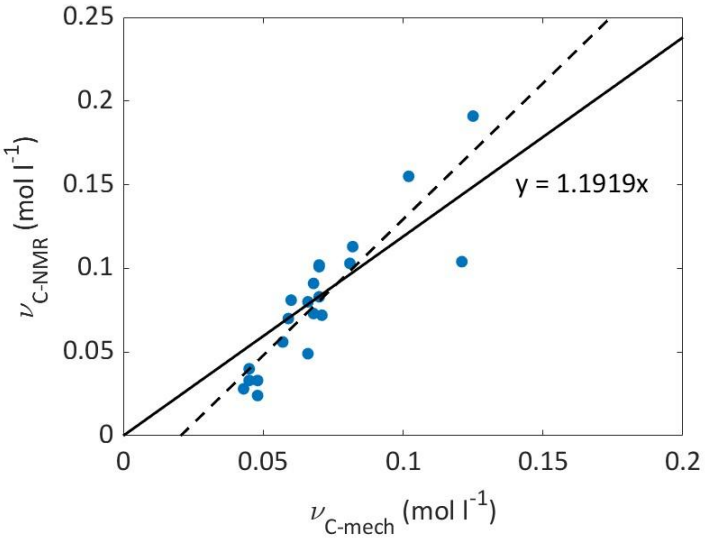

Figure 10. $\nu_{C\text{-}NMR}$ values obtained by 1H DQ NMR measurements as a function of ν_C computed from the Young's modulus at small deformations according to the affine model for all non-aged and aged PDMS. The dashed and solid lines are linear fits serving as a guide for the eyes.

It is observed that for each PDMS, a trend between both data (i.e. mechanical testing and DQ NMR) is obtained. Two interpretations can be proposed:

- a linear fit with a zero intersect at the origin (Figure 10)

- a linear fit (represented by dashed lines) with an intersect higher than 0 when $\nu_{C\text{-}NMR}$ = 0. The following explanation can be proposed: in theory, if there are no chemical crosslinks, the crosslink density would be of zero. However physical entanglements act as effective crosslinks within polymers. The difference between both measurements, i.e. the non-zero x-intercept, is the timescale at which the materials are probed. Mechanical testing occurs at characteristic times of 1 s whereas DQ NMR probes the sample at characteristic times of 1 ms. Chemical crosslinks are probed at both timescales, however physical entanglements are only probed at small timescales, indeed at 1s such entanglements have relaxed. Thus, DQ NMR is more sensible to characterize chemical and physical crosslink nodes, with the non-zero x-intercept being the amount of physical crosslinks in these PDMS formulations. Indeed, for low-crosslinked polymers such as the PDMS studied herein, it might be possible that the critical percolation threshold has been reached. In theory, for elastic crosslinked chains, the elastic modulus E can be equated as $E=k_BTV$ where k_B is Bolzmann's constant, T is the

temperature and V is the volume of elastically crosslinked chains, as stated in [37] (and references cited therein). In such a case, no x-intercept or y-intercept should be observed. The functionality threshold fc is estimated to be of ca. 3. Below this functionality threshold, the network becomes floppy and the elastic modulus starts to vanish (i.e. non-zero x-intercept), even though chains are still topologically connected [37] (and references cited therein). Nevertheless, it is important to point out that, when all results are plotted together in Figure 10, a mastercurve is observed for all PDMS, non-aged or aged. This means that a correlation between the variation of crosslink density probed at the molecular scale by DQ NMR and the macroscopic mechanical modulus measured by tensile tests. In other words, a direct link between the increase or breaking of crosslink nodes with the materials behavior has been established.

Finally, to relate the molecular mobility to the macroscopic properties of PDMS samples, the relaxation time τ obtained from fitting the I_{ref} NMR signals according to Equation 7 was plotted as a function of the crosslink density v in Figure 11. Such correlations between the NMR relaxation times determined from Carr-Purcell-Meiboom-Gill sequences and the concentration in elastically active chains have been previously discussed in polyester urethane networks [58]. Nevertheless, such an approach has never been undertaken on aged polymer samples.

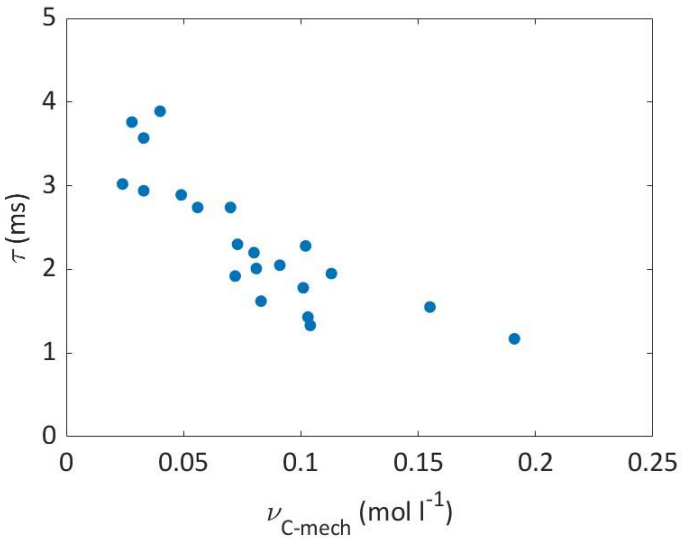

Figure 11. Effect of elastically active chains concentrations (from the $3C_1 + 4.5C_2$ quantity) on NMR DQ relaxation time τ.

It is seen in Figure 11 that a trend between and is observed. When the crosslink density increases, the relaxation time decreases. This is due to the fact that during crosslinking, chains become more constrained (i.e. less mobile), as such they would tend to relax faster than in the case of non-aged samples. This approach could also be treated as a starting point for a new method determining the evolution of elastically active chains concentration as a function of polymer aging in future works.

CONCLUSIONS

In this work, three systems made of unfilled Room Temperature Vulcanized PDMS were synthesized, with crosslinks density ranging from 0.028 to 0.120 mol kg^{-1} corresponding to shore A values ranging

to 10 to 42. They were either thermally aged at 250°C under air or submitted to an aminolysis ageing. Samples were systematically characterized by mechanical tests (uniaxial tensile tests), sol gel analysis and Double Quantum NMR. Data were exploited to extract the concentration in elastically active chains. Thermal ageing was shown to induce some chain scissions in the early degradation times, but crosslinking becomes predominant after 24h ageing at 250°C. Samples degraded by aminolysis exhibit a behavior attributed to a moderate chain scission process. Stress strain curves were modelled by a so-called Ogden model with two contributions, respectively associated to long and short elastically active chains, the first being favored by chain scissions and the second by crosslinking process. Despite the semi-empirical nature of such hyperelastic model, the parameters were tentatively justified from their correlation with NMR data and exploited to propose a multiscale prediction of embrittlement of PDMS networks.

REFERENCES

1. A. Naderian Jahromi, Edward A. Cherney, Shesha H. Jayaram. Aging Characteristics of RTV Silicone Rubber Insulator Coatings. IEEE Transactions on Dielectrics and Electrical Insulation, Volume 15, Issue 2, April 2008, 444-452.

2. J.A. Smith, S. Li, E. Mele, A. Goulas, D. Engstrøm, V. V. Silberschmidt. Printability and mechanical performance of biomedical PDMS-PEEK composites developed for material extrusion. Journal of the Mechanical Behavior of Biomedical Materials, Volume 115, 2021, 104291.

3. E.J. Kappert, M.J.T. Raaijmakers, K. Tempelman, F.P. Cuperus, W. Ogieglo, N.E. Benes. Swelling of 9 polymers commonly employed for solvent-resistant nanofiltration membranes: A comprehensive dataset. Journal of Membrane Science, Volume 569, 2019, 177-199.

4. J. Ng Lee, C. Park, G.M. Whitesides. Solvent Compatibility of Poly(dimethylsiloxane)-Based Microfluidic Devices. Analytical Chemistry, Volume 75, Issue 23, 2003, 6544–6554.

5. B. Ameduri, B. Boutevin. Update on fluoroelastomers: from perfluoroelastomers to fluorosilicones and fluorophosphazenes. Journal of Fluorine Chemistry, Volume 126, Issue 2, 2005, Pages 221-229.

6. N. Grassie, I.G. Macfarlane. The thermal degradation of polysiloxanes—I. Poly(dimethylsiloxane). European Polymer Journal, Volume 14, Issue 11, 1978, Pages 875-884.

7. G. Camino, S.M. Lomakin, M. Lazzari. Polydimethylsiloxane thermal degradation Part 1. Kinetic aspects. Polymer, Volume 42, Issue 6, 2001, Pages 2395-2402.

8. Y. Israeli, J. Lacoste, J. Cavezzan, J. Lemaire. Photooxidation of polydimethylsiloxane oils and resins. IV—effect of phenyl groups. Polymer Degradation and Stability, Volume 47, Issue 3, 1995, Pages 357-362.

9. J.D. Jovanovic, M.N. Govedarica, P.R. Dvornic, I.G. Popovic. The thermogravimetric analysis of some polysiloxanes. Polymer Degradation and Stability, Volume 61, Issue 1, 1998, Pages 87-93.

10. A. Labouriau, C. Cady, J. Gill, J. Stull, D. Ortiz-Acosta, K. Henderson, V. Hartung, A. Quintana, M. Celina. Gamma irradiation and oxidative degradation of a silica-filled silicone elastomer. Polymer Degradation and Stability, Volume 116, 2015, Pages 62-74.

11. R.S. Maxwell, R. Cohenour, W. Sung, D. Solyom, M. Patel. The effects of γ-radiation on the thermal, mechanical, and segmental dynamics of a silica filled, room temperature vulcanized polysiloxane rubber. Polymer Degradation and Stability, Volume 80, Issue 3, 2003, Pages 443-450.

12. T.-M. Durďáková, Z. Hrdlička, M. Král, Š. Hovorka, A. Vögele, R. Eichler, P. Trtik, O. Vopička. Radiation softening and hardening of PDMS in combined neutron and γ rays. Polymer Degradation and Stability, Volume 208, 2023, 110241.

13. A. Shefer, M. Gottlieb. Effect of crosslinks on the glass transition temperature of end-linked elastomers. Macromolecules, Volume 25, Issue 15, 1992, Pages 4036–4042.

14. M. Demleitner, F. Hübner, A. Mainz, H. Ruckdäschel, V. Altstädt, L. Michely, A. Rios de Anda. Influence of network structure determined by Time-domain 1H Double Quantum NMR on the creep properties of non-stoichiometric epoxy-amine resins aimed for chemical anchoring applications. Polymer, Volume 286, 2023, 126373.

15. A.P. Munaro, G.P. da Cunha, J.G. Filgueiras, J.M. Pinto, M. Munaro, E.R. de Azevedo, L.C. Akcelrud. Ageing and structural changes in PDMS rubber investigated by time domain NMR. Polymer Degradation and Stability, Volume 166, 2019, Pages 300-306.

16. R.J. Pazur, A. Tilley, B. Zaman, C. Porter. Investigating the heat resistance of peroxide‐cured silicone rubber for shelf and service life considerations. Polymer Bulletin 81, 2024, 12867–12891.

17. L. Bernardi, R. Hopf, A. Ferrari, A.E. Ehret, E. Mazza. On the large strain deformation behavior of silicone-based elastomers for biomedical applications. Polymer Testing, Volume 58, 2017, Pages 189-198,

18. M. Englert, F. Minister, A. Moussaoui, W. Pisula. Mechanical properties of thermo-oxidative aged silicone rubber thermally stabilized by titanium oxide based fillers. Polymer Testing, Volume 115, 2022, 107726.

19. D. Oldfield, T. Symes. Long term natural ageing of silicone elastomers. Polymer Testing, Volume 15, Issue 2, 1996, Pages 115-128.

20. H. Zhang. The Permeability Characteristics of Silicone Rubber. 2006 SAMPE Fall Technical Conference, "Global Advances in Materials and Process Engineering", proceedings, Coatings and Sealants Section, November 6 – 9, 2006, Dallas, TX.

21. J. Baum, M. Munowitz, A.N. Garroway, A. Pines. Multiplequantum dynamics in solid state NMR. The Journal of Chemical Physics Volume 83, Issue 5, 1 September 1985, pages 2015–2025.

22. J. Baum, A. Pines. NMR studies of clustering in solids. Journal of the American Chemical Society, Volume 108, Issue 24, 1986, 7447–7454.

23. K. Saalwächter, P. Ziegler, O. Spyckerelle, B. Haidar, A. Vidal, J.U. Sommer. 1H multiple-quantum nuclear magnetic resonance investigations of molecular order distributions in poly(dimethylsiloxane) networks: Evidence for a linear mixing law in bimodal systems. The Journal of Chemical Physics, Volume 119, 2003, Pages 3468–3482.

24. K. Saalwächter, 1H multiple-quantum nuclear magnetic resonance investigations of molecular order in polymer networks. II. Intensity decay and restricted slow dynamics. The Journal of Chemical Physics, Volume 120, 2004, 454–464.

25. K. Saalwächter, F. Kleinschmidt, J.-U. Sommer. Swelling heterogeneities in end-linked model networks: A combined proton multiple-quantum NMR and computer simulation study. Macromolecules, Volume 37, 2004, Pages 8556–8568.

26. K. Saalwächter, B. Herrero, M.A. López-Manchado. Chain order and crosslink density of elastomers as investigated by proton multiple-quantum NMR. Macromolecules, Volume 38, 2005, Pages 9650–9660.

27. K. Saalwächter. Proton multiple-quantum NMR for the study of chain dynamics and structural constraints in polymeric soft materials. Progress in Nuclear Magnetic Resonance Spectroscopy, Volume 51, Issue 1, August 2007, Pages 1-35.

28. W. Chassé, S. Schlögl, G. Riess, K. Saalwächter. Inhomogeneities and local chain stretching in partially swollen networks. Soft Matter, Volume 9, Issue 29, 2013, Pages 6943–6954.

29. K. Saalwächter, A. Heuer. Chain dynamics in elastomers as investigated by proton multiple-quantum NMR. Macromolecules, Volume 39, Issue 9, 2006, 3291–3301.

30. F.V. Chávez, K. Saalwächter. Time-domain NMR observation of entangled polymer dynamics: Analytical theory of signal functions. Macromolecules, Volume 44, Issue 6, 2011, Pages 1560–1569.

31. C. Lorthioir, S. Randriamahefa, B. Deloche. Some aspects of the orientational order distribution of flexible chains in a diblock mesophase. The Journal of Chemical Physics, Volume 139, Issue 22, 2013, 224903.

32. B. Gabrielle, C. Lorthioir, F. Lauprêtre, Thermal aging of interfacial polymer chains in ethylene-propylene-diene terpolymer/aluminum hydroxide composites: Solid-state NMR study, The Journal of Physical Chemistry B, Volume 115, 2011, Pages 12392–12400.

33. L.D. Landau, E.M. Lifshitz, J.B. Sykes, W.H. Reid, Ellis H. Dill. Theory of elasticity: Vol. 7 of course of theoretical physics. Physics Today Volume 13, Issue 7, 1960, 44–46.

34. L.R.G. Treloar, D.J. Montgomery. The physics of rubber elasticity. Physics Today, Volume 12, Issue 2, 1959, 32–34.

35. B. van Bochove, S. Spoljaric, J. Seppälä, A. Rios de Anda. Multiscale structural characterization of biocompatible poly(trimethylene carbonate) networks photo-cross-linked in a solvent. Polymer Testing, Volume 90, 2020, 106740.

36. A. Vieyres, R. Pérez-Aparicio, P.A. Albouy, O. Sanseau, K. Saalwächter, D.R. Long, P. Sotta. Sulfur-cured natural rubber elastomer networks: Correlating cross-link density, chain orientation, and mechanical response by combined techniques. Macromolecules, Volume 46, Issue 3, 2013, 889–899.

37. B. Van Bochove, S. Spoljaric, J. Seppälä, P. Sotta, A. Rios De Anda. Multiscale structural characterization of biocompatible poly(trimethylene carbonate) photoreticulated networks. ACS Applied Polymer Materials Volume 1, Issue 7, 2019, 1811–1820.

38. A. Rios De Anda, P. Sotta, T. Modjinou, V. Langlois, D.L. Versace, E. Renard. Multiscale structural characterization of biobased diallyleugenol polymer networks. Macromolecules, Volume 53, Issue 6, 2020, 2187–2197.

39. M. Martin-Gallego, A. González-Jiménez, R. Verdejo, M.A. Lopez-Manchado, J. Lopez Valentin. Epoxy resin curing reaction studied by proton multiple-quantum NMR. Journal of Polymer Science Part B Polymer Physics Volume 53, Issue 18, September 2015, Pages 1324-1332.

40. F. Hübner, E. Szpoganicz, M. Demleitner, J. Kuhnigk, V. Altstädt, A. Rios De Anda. Time domain 1H NMR, thermomechanical, and rheology multiscale structural characterization of polydimethylsiloxane toughened epoxy nanocomposites for liquid composite molding. ACS Applied Polymer Material Volume 2, Issue 11, 2020, 4779–4789.

41. N. Mattar, F. Hübner, M. Demleitner, A. Brückner, V. Langlois, E. Renard, H. Ruckdäschel, A. Rios De Anda. Multiscale characterization of creep and fatigue crack propagation resistance of fully biobased epoxy-amine resins. ACS Appl. Polym. Mater Volume 3, Issue 10, 2021, 5134–5144.

42. N. Mattar, E. Renard, V. Langlois, A. Rios de Anda. Multiscale network structure analysis by time domain 1H DQ NMR and DMA of resorcinol diglycidyl ether-jeffamine matrices. ChemistrySelect, Volume 5, Issue 36, September 30, 2020, Pages 11291-11298.

43. P.W. Anderson, P. R. Weiss. Exchange Narrowing in Paramagnetic Resonance. Reviews of Modern Physics, Volume 25, Issue 1, 1953, 269-276.

44. A. Papon, K. Saalwächter, K. Schäler, L. Guy, F. Lequeux, H. Montes. Low-Field NMR Investigations of Nanocomposites: Polymer Dynamics and Network Effects. Macromolecules, Volume 44, Issue 4, 2011, 913–922.

45. P.J. Flory, J. Rehner Jr. Statistical Mechanics of Cross-Linked Polymer Networks II. Swelling. The Journal of Chemical Physics Volume 11, 1943, Pages 521-526

46. W. Chassé, M. Lang, J.U. Sommer, K. Saalwächter. Cross-Link Density Estimation of PDMS Networks with Precise Consideration of Networks Defects. Macromolecules, Volume 45, Issue 2, 2012, Pages 899-912.

47. Q. Xu, M. Pang, L. Zhu, Y. Zhang, S. Feng. Mechanical properties of silicone rubber composed of diverse vinyl content silicone gums blending. Materials & Design Volume 31, Issue 9, October 2010, Pages 4083-4087.

48. Q. Hao, Z. Malhi, P.M. François, E. Richaud. Hyperelasticity modelling for thermally aged silicones. Polymer Bulletin Volume 81, 2024, 1249–1268.

49. J.-F.Masson, I. Lopez–Carreon, J. Wu, O. Obukohwo, P. Collins, M. Riahinezhad, E. Esmizadeh. Degradation and service-life prediction of silicone rubber in a highly alkaline environment simulating concrete Engineering Failure Analysis 138, 2022, 106305.

50. C. Batich, D. DePalma, J. Marotta, G. Latorre. Silicone Degradation Reactions. Part of the Current Topics in Microbiology and Immunology book series (CT MICROBIOLOGY,volume 210). Conference paper 466, 13–23

51. Q. De Monléon, P. Banet, L. Chikh, O. Fichet. Effects of pyromellitidiimide pattern on thermomechanical properties and thermal stability of silicone networks. Polymer Degradation and Stability 206, 2022, 110187.

52. C.-L. Chang, T.-M. Don, H. Shih-Jen Lee, Y.-O. Sha. Studies on the aminolysis of RTV silicone rubber and modifications of degradation products. Polymer Degradation and Stability, Volume 85, Issue 2, 2004, Pages 769-777.

53. S.P. Pappas, R.L. Just. Aminolysis of crosslinked polysiloxanes: tautomeric catalysis by 2-pyridone. Journal of Polymer Science. Part A-1, Polymer Chemistry, Volume 18, Issue 2, 1980, Pages 527-531.

54. R.W. Ogden. Large deformation isotropic elasticity – on the correlation of theory and experiment for incompressible rubberlike solids. Proc Roy Soc A 326: (1972) 565–584. https://doi.org/10.1098/rspa.1972.0026

55. P.J. Flory. Molecular Theory of Rubber Elasticity. Polymer Journal, Volume 17, Issue 1, 1985, Pages 1-12.

56. L. Bernardi, R. Hopf, A. Ferrari, A.E. Ehret, E. Mazza. On the large strain deformation behavior of silicone-based elastomers for biomedical applications. Polymer Testing, Volume 58, 2017, 189-198.

57. M.A. Llorente, A.L. Andrady, J.E. Mark. Model networks of end-linked polydimethylsiloxane chains. XI. Use of very short network chains to improve ultimate properties. Journal of Polymer Science Polymer Physics Volume 19, Issue 4, 1981, Pages 621-630.

[58] E. Richaud, I. Derue, P. Gilormini, J. Verdu, C. Vaulot, M. Coquillat, N. Desgardin, A. Vandenbrouke. Plasticizer effect on network structure and hydrolytic degradation. European Polymer Journal, Volume 69, 2015, Pages 232-246.